A Novel Boron-rich Scandium Borocarbosilicide; $Sc_{0.83-x}B_{10.0-y}C_{0.17+y}Si_{0.083-z}$ (x = 0.030, y = 0.36 and z = 0.026): Floating Zone Crystal Growth and Structure Analysis

Takaho Tanaka* and Akira Sato

Advanced Materials Laboratory, National Institute for Materials Science, Namiki 1-1, Tsukuba, Ibaraki 305-0044, Japan

Keywords; $Sc_{0.83-x}B_{10.0-y}C_{0.17+y}Si_{0.083-z}$, boron-rich scandium borocarbosilicide, floating zone crystal growth, single-crystal structure analysis, face-centered cubic structure, B_{10} polyhedron, B_{12} icosahedron,

Abstract

Single crystals of a novel boron-rich scandium borocarbosilicide $Sc_{0.83-x}B_{10.0-y}C_{0.17+y}Si_{0.083-z}$ were grown by the floating zone method using a four-xenon lamp mirror-type image furnace. Structure analysis using single-crystal X-ray diffraction data showed that $Sc_{0.83-x}B_{10.0-y}C_{0.17+y}Si_{0.083-z}$ has a face-centered cubic with lattice constant a = 2.03085 nm and space group of F43m. The crystal composition calculated from the structure analysis was $ScB_{12.0}C_{0.65}Si_{0.071}$ which agreed with the measured composition of $ScB_{12.7}C_{0.62}Si_{0.08}$. In the crystal structure which is a new structure type of boron-rich borides, there are three structurally independent B_{12} icosahedra I(1), I(2) and I(3) and one B_{10} polyhedron which interconnect each other to form a three-dimensional boron framework. There are four fully occupied bridging sites, one is the C site and other three sites are occupied statistically by B or C. The Sc atoms reside three interstitial sites of the boron framework. Two Si sites are tetrahedrally surrounded by the bridging carbon sites and by the bridging boron/carbon mixed occupation sites, respectively. The boron framework structure can be understood more easily by introducing larger structure units, they are a super tetrahedra T(1) made up by four icosahedra I(1), a super tetrahedra T(2) made up by four icosahedra I(2) and a super octahedra O(1) made up by six icosahedra I(3).

1. Introduction

In our previous paper, we reported subsolidus phase relations in the ternary Sc-B-C system [1] where many new phases were identified especially in boron-rich part of the phase relation, namely ScB_{19}, $ScB_{17}C_{0.25}$, $ScB_{15}C_{0.8}$ and $ScB_{15}C_{1.26}$. For most of them, we could determine their crystal structures (ScB_{19} [2, 3], $ScB_{17}C_{0.25}$ [4, 5], $ScB_{15}C_{1.26}$ [6]) up to now; however, for $ScB_{15}C_{0.8}$ even indexing of powder data was unsuccessful because of weak peak intensities and the complicated powder pattern. All these phases decompose at high temperatures without melting, thus single-crystal growths from the melt phase are impossible. Single crystals of $ScB_{17}C_{0.25}$ and $ScB_{15}C_{1.26}$ phases could be successfully obtained by the high-temperature solution growth method using metal fluxes like Cu, Si and Sn. On the other hand, following the crystal growth of YB_{50} [7], the Si addition method was successfully applied to grow crystals of ScB_{19} as a form of scandium borosilicide $ScB_{19+x}Si_y$ using the melt growth method, where Si addition is effective to lower melting temperature and increase phase stability, resultantly the Si-doped ScB_{19} phase could coexist with the melt phase without decomposing [3].

We expected the Si addition method to be useful for growing crystals of some of these scandium borocarbides. Surprisingly, crystals of the $ScB_{15}C_{0.8}$ phase which is the most uninvestigated phase because of lack of single crystals could be grown by the method. In the present paper, the floating zone crystal growth of $Sc_{0.83-x}B_{10.0-y}C_{0.17+y}Si_{0.083-z}$ which is the Si-added $ScB_{15}C_{0.8}$ phase and single-crystal structure analysis are presented.

2. Experimental

2.1. Floating zone crystal growth

Raw powders of ScB_x were synthesized by a borothermal reduction method using powder of Sc_2O_3 (3N, Crystal Systems Inc., Japan) and amorphous boron (3N, SB-Boron Inc., USA). The reaction was carried out in a boron nitride crucible inserted in a graphite susceptor using a RF heating furnace under vacuum for several hours at about 1700°C. After mixing suitable amount of B_4C powder (3N, Koujundo Kagaku Inc., Japan) and SiB_6 powder (98%, Cerac Inc., USA) which were used as carbon and silicon sources, respectively, the powder was pressed into a green rod by cold isostatic press (CIP) process at 250 MPa and was sintered in the same way as that used for the ScB_x synthesis. The density of the sintered rod stayed at about 60% of theoretical value. In order to densify the rod and to achieve nearly 100% density, the rod was horizontally zone melted on a half-cut BN pipe put on a groove of a water-cooled copper plate under Ar gas atmosphere using a xenon lamp image furnace. After several times zone melting through the rod changing the sweep direction it became a rather smooth and dense rod with dimensions of about 6 mm in diameter and 100 mm long.

Floating zone crystal growth was carried out using a four-xenon lamp-ellipsoidal mirror-type image furnace. The feed rod and the seed rod were set on the upper and lower axis, respectively. A small piece of Si was put on the top of the seed rod. When the Si piece started to melt, the bottom of the feed rod was touched to the Si melt, then gradually temperature was raised up

increasing the volume of the molten zone by dissolving the bottom part of the feed rod into the molten zone. After a suitable zone volume was achieved, the floating zone crystal growth was started by driving downwards both the feed rod and the seed rod synchronously at a rate of 5 mm/h. Both rods were counter rotated at ±35 rpm and the atmosphere was flowing Ar.

2.2. Chemical analysis

For chemical analysis, the crystal was crushed to a powder by a stainless-steel mortar and the stainless steel contamination was washed by a dilute HCl solution and rinsed away. The obtained powder was dissolved into a conc.HNO_3/conc.HCl (1:1) solution keeping it at 150°C for 16 h in an air tight capsule. Using the solution, scandium, boron and silicon contents were determined by an inductively coupled plasma atomic emission spectroscopy. Carbon content was determined by a volumetric combustion method using a carbon determinator (WR-12, Leco Co., USA). Standard deviation of the chemical analysis was within ±2% for each element.

Crystal composition was also measured by an EPMA equipment (JXA-8600MX, JEOL Co., Japan) using standards of a single-crystal ScB_{12} for Sc and B, a single-crystal $B_{4.5}C$ for C and a single-crystal SiC for Si. Standard deviations of the EPMA measurement were ±2% for Sc, ±1% for B, ±5% for C and ±9% for Si, respectively.

2.3. X-ray diffraction

Phase identification was carried out using a standard powder X-ray diffractometer (R-2000, Rigaku Co., Japan) with CuKα radiation. The X-ray single-crystal data were collected on an Enraf-Nonius CAD4 automatic 4-circle diffractometer with graphite monochromated MoKα radiation. Crystal data and intensity measurement data are given in Table 1.

Table 1. Crystallographic and data collection parameters

Crystal composition	$ScB_{12.7}C_{0.62}Si_{0.08}$ (Obtained by chemical analysis)
Crystal system	Face-centered cubic
Space group	*F*43m (No.216)
Lattice constant (nm)	2.03085(5)
Unit-cell volume (nm^3)	8.376
Structural formula	$19.3Sc{\cdot}10B_{12}{\cdot}4(B_{10.7}C_{1.3}){\cdot}6B_{10}{\cdot}4(B_{2.1}C_{0.91}){\cdot}4C{\cdot}1.4Si$
Chemical composition	$ScB_{12.0}C_{0.65}Si_{0.071}$ (Obtained by structure analysis)
Z	4
D_x (g/cm^3)	2.824
D_m (g/cm^3)	2.819
μ for MoK*a* (cm^{-1})	15.43
Crystal dimensions (mm)	0.30 x 0.30 x 0.20
Reflection measured	$0 \leqq h \leqq 32, 0 \leqq k \leqq 32, 0 \leqq l \leqq 32$
$2\theta_{max}$	70°
Structure refinement program	SHELXL97
R1	0.048 ($Fo>4\sigma(Fo)$, for 941 *F*o), 0.050 (all *F*o, for 980 *F*o)
wR2	0.126 (*F*2)
Number of variables	84

The intensity data were corrected for Lorenz and polarization effects. The absorption correction applied to the collected data was empirical based on Ψ-scans.

3. Results and discussion

3.1. Crystal growth

The first zone pass trial was carried out using a feed rod with composition of $ScB_{15}C_{1.26}Si_{1.0}$ expecting that an $ScB_{15}C_{1.26}$ phase crystal can be grown by the Si addition method. The zone pass was quite unstable and after only about 10 mm zone pass further zone pass became impossible. The obtained rod included so many small cracks and only the central region of about 2 mm diameter seemed to be a crystal. Powder XRD analysis for the central region indicated unexpectedly the existence of the $ScB_{15}C_{0.8}$ phase with some unknown phases. Thus, the second zone pass trial was carried out using a feed rod with a composition of $ScB_{15}C_{0.8}Si_{1.0}$. Stability of the zone pass was not so improved. When the molten zone was gradually cooled down after about 15 mm zone pass, its freezing behavior indicated the existence of excess free Si in it. For both the trials, the molten zone was formed by only melting the feed rod without adding an additional Si piece. The excess free Si in the molten zone after the rather short zone pass meant that the Si content in the feed rod was very high. By reducing the Si content in the feed rod by half of the second one the third zone pass trial could increase the central crystal region. Chemical analysis showed that the composition of the central crystal region was $ScB_{15.1}C_{0.89}Si_{0.22}$. Most of the powder XRD peaks could be assigned by a face-centered cubic structure with a lattice constant of a = 2.0309 nm and an additional B_4C.

We cracked the central crystal part and picked up several crystal pieces for single-crystal structure analysis. Fortunately, one of them showed high quality sufficient for single-crystal data collection. However, preliminary structure analysis showed a composition ratio [B+C]/[Sc] ~13 which was very small as compared with the chemical composition value [B+C]/[Sc] ~16. Further structure refinement could neither find more B or C atom sites nor reduce Sc site occupancies. Thus, we carried out EPMA analysis for sister crystals, the resulting chemical compositions (~ $ScB_{12.5}C_{0.8}Si_{0.06}$) were comparable to that estimated from the structure refinement.

According to the above results, further crystal growths were tried gradually reducing B+C content in the feed rods. In these cases a small Si piece was inserted between the feed rod and the seed rod in order to adjust the Si content in the molten zone as mentioned in the previous section. In higher B+C content cases a small amount of precipitation could be microscopically observed on the polished surface of the cross section of the crystal. The precipitation was identified as B_4C crystallites by EPMA analysis. Thus, further reduction of the B+C content should give a single phase, but surprisingly two new phases appeared occasionally at the nominal feed rod compositions around $ScB_{12.5}C_{0.7}Si_{0.07}$, especially at the initial stage of crystal growth where the steady crystal growth condition has not been established yet. Fortunately, a single-phase crystal of both two phases could be taken out from their large crystallites. One has a hexagonal crystal structure with lattice constants of a=1.4363(4) nm and c=2.3576(13) nm and space group P6m2 (No.187). Its composition given by EPMA analysis was $ScB_{11.7}C_{0.6}Si_{0.04}$. Another has an

orthorhombic crystal structure with lattice constants of a=1.7296(2) nm, b=1.6059(2) nm and c=1.4471(1) nm and space group Pbam (No.55) and its composition was $ScB_{12.8}C_{0.7}Si_{0.004}$. Structure analyses of both phases will be given elsewhere in future.

More than 10 mm cubic phase crystals could be grown although the zone passed rods often included the hexagonal phase. However, the zone passed rods consisted of 2 ~ 3 mm size grains. During every zone pass, the molten zone had a strongly constricted shape which could not be moderated by heating power adjustments and many grains were observed to nucleate successively on the surface of the growing crystals. Actually such nucleation has occurred even inside of the crystal.

The grown crystal is shown in Fig. 1. Chemical analysis results of the crystal are summarized in Table 2. Although the composition difference between the middle part and the z-end part is fairly small, the middle part has included a large amount of the hexagonal phase and the z-end part has included little, which indicates that the composition control is very delicate in order to obtain single phase crystals.

Fig. 1. An example of $Sc_{0.83-x}B_{10.0-y}C_{0.17+y}Si_{0.083-z}$ crystal.

Table 2. Chemical composition of an FZ-grown crystal

Position	Composition
feed rod	$ScB_{13.3}C_{0.65}Si_{0.066}$
zone	$ScB_{9.9}C_{0.39}Si_{0.23}$
z-end (crystal)	$ScB_{12.3}C_{0.57}Si_{0.071}$
middle (crystal)	$ScB_{12.3}C_{0.53}Si_{0.067}$
initial (crystal)	$ScB_{14.3}C_{0.78}Si_{0.104}$
Partition coefficients at the growth interface	
Element	Partition coefficient
Si	~ 0.26
C	~ 1.2

Powder XRD pattern of the single-phase crystal was compared with that of $ScB_{15}C_{0.8}$ powder synthesized by solid-state reaction. Although some extra peaks could be observed in the diffraction pattern of $ScB_{15}C_{0.8}$, especially at low-angle region both diffraction patterns agreed well, we concluded that they are isostructural. If Sc content in the crystal is reduced to 80% without changing B and C contents, the composition would agree with the powder composition $ScB_{15}C_{0.8}$ suggesting that the Sc site occupancy in the powder is 20% lower than that in the crystal. It should be noted here, when the powder with composition of about $ScB_{12.5}C_{0.8}$ was synthesized by solid-state reaction in order to produce a feed rod for the FZ crystal growth, it was not the cubic phase but the orthorhombic phase. The FZ crystal growth using the feed rod could grow the orthorhombic phase only at the initial stage of the crystal growth where the molten zone was at comparatively low temperature because of the addition of a rather large piece of Si in order to forming the molten zone easily. Till now we are not successful to keep such large amount of Si during zone pass and the Si content in the molten zone gradually decreased as the molten zone passed, resultantly the temperature of the molten zone increased and the cubic phase appeared. However, this seems to contradict to the fact that the orthorhombic phase has less Si content than that of the cubic phase so that once the orthorhombic phase appeared during the FZ crystal growth using a feed rod for the cubic phase growth, Si must accumulate in the molten zone and the orthorhombic phase should grow continuously. More precise phase analysis must be done.

Partition coefficient is normally used as a measure of how much an impurity element is rejected or introduced to a crystal through growth interface, however, this concept can be applied to a minor constituent element also. Depending on whether the partition coefficient of the element is larger or smaller than unity, the melting temperature would increase or decrease, respectively. Partition coefficients of Si and C can be calculated as a ratio between their content in the zone end crystal and that in the molten zone. For the present cubic phase, they are about 0.26 and 1.2, respectively, as listed in Table 2. Thus their behaviors are opposite, i.e., Si acts to reduce the melting temperature and C increases.

Since the molten zone composition is fairly different from the composition of the growing crystal not only for Si and C but also for B, crystal growth mode is closer to the high-temperature solution growth with self-flux than the melt growth. Probably, this is a reason of continuous nucleation during the zone pass, much slower growth rate would be preferable in order to obtain a single grain crystal.

3.2. Structure analysis

Single-crystal specimens for 4-circle XRD data collection were obtained by cracking a part of the FZ-grown crystals and the part remained was sent to chemical analysis. Two measurements were done using different crystals, one was picked up from a crystal grown at an early stage using a feed rod with composition of $ScB_{15}C_{0.8}Si_{1.0}$. Another was picked up from a crystal grown later using a feed rod whose composition was adjusted to that obtained by the first structure analysis. Although the overall crystal quality of the latter mother crystal was much better, both crystal specimens have had sufficiently high qualities for data collection. The obtained results were

almost same except for small differences of B/C mixed occupancies at several sites.

An initial structure solution was obtained by SIR92 [8] according to the space group *F*43m and the program SHELXL-97 [9] was used for refinement. The direct method gave 26 atomic positions in which three Sc sites, one Si site, two C sites and 20 B sites were assigned. Examination of the bond distances suggested that some C and B sites should be exchanged and one B site should be reassigned to an additional Si site; thus, three Sc sites, two Si sites, one C site and 20 B sites are counted in the $Sc_{0.83-x}B_{10.0-y}C_{0.17+y}Si_{0.083-z}$ crystal structure. Visualization of the crystal structure using the graphic program CrystalMaker [10] immediately showed a three-dimensional boron framework composed of interconnected B_{12} icosahedra and B_{10} polyhedra, where 17 B sites are used to construct structurally independent three boron icosahedra and one B_{10} polyhedron. The remaining three B sites and the C site are bridging sites, which link the icosahedra and B_{10} polyhedron. Sc atoms reside in voids of the boron framework. Two Si sites are tetrahedrally surrounded by the bridging carbon sites and by the bridging boron/carbon mixed occupation sites, respectively. The structure refinement for the first specimen gave slightly better *R* values than that for the second specimen, i.e., for the first specimen the final refinement of 84 parameters for 941 independent reflections ($Fo>4\sigma(Fo)$) resulted in an *R1* value of 4.8% and 5.0% for all 980 independent reflections and for the second specimen an *R1* value of 5.0% for 930 independent reflections ($Fo>4\sigma(Fo)$) and 5.5% for all 979 independent reflections.

Compositions of both specimens obtained by the structure refinements were $Sc_{0.80}B_{9.6}C_{0.52}Si_{0.057}$ ($=ScB_{12.0}C_{0.65}Si_{0.071}$) and $Sc_{0.78}B_{9.6}C_{0.56}Si_{0.062}$ ($=ScB_{12.3}C_{0.71}Si_{0.079}$), respectively. They are very close each other, the latter one has slightly less Sc, same B and more C and Si contents than the former one. The final atomic coordinates, occupancy factors and temperature factors for the first specimen are listed in Table 3 and the inter atomic distances are summarized in Table 4.

B(1)-B(4), B(5)-B(8), B(9)-B(13) and B(14)-B(17) form the icosahedra I(1), I(2), I(3) and the B_{10} polyhedron, respectively. The B_{10} polyhedron which has not been observed previously in any boron-rich borides is shown in Fig. 2 and consists of 10 boron atoms. One side of the polyhedron has a house roof-like shape formed by two rectangles and another side of the polyhedron is a half-part of icosahedron. B,C(18)- B,C(20) and C(1) sites are bridging sites.

Mixed occupancy between B and C on all bridging sites were examined. The result showed that the C(1) site is occupied only by carbon and other sites are occupied by both. A monotonic relation between B occupancy ratios and bond lengths can be seen as listed in Table 4, a higher B occupancy ratio corresponds to a longer bond length. For the B,C(18) site of the second specimen, B/C occupancy ratio of 0.88/0.12 is much higher than that (0.51/0.49) of the first specimen, resultantly the bond distance increases to 1.757(7) Å from 1.747(7) Å. The other two bridging sites of both specimens have same B/C occupancy ratios and same bond distances.

Since the B,C(6) site in the icosahedron I(2) has also very short bond lengths of 1.615(10) Å for intericosahedron bond and of 1.714(9)Å for intraicosahedron bond, mixed occupancy between B and C was also examined for this site. The B/C ratio is 0.58/0.42 as shown in Table 3. As shown in Fig. 3, four I(2) icosahedra arrange each other tetrahedrally. The tetrahedron which consists of four I(2) icosahedra is now referred as a super tetrahedron T(2). At the center of the

super tetrahedron T(2), 12 B,C(6) sites form a polyhedron cluster composed of four hexagonal rings and four triangles where about 7B and 5C are accommodated. For the second specimen, the B/C occupancy ratio for the

B,C(6) site is reversed to B/C=0.39/0.61 causing shorter bond lengths of 1.605(10) and 1.710(9) Å, respectively. About 5B and 7C are accommodated on the 12 B,C(6) site polyhedron. Thus carbon atoms localize in the $Sc_{0.83-x}B_{10.0-y}C_{0.17+y}Si_{0.083-z}$ crystal structure forming clusters.

Table. 3. Final atomic coordinates, occupancy factors and temperature factors

Atom	Site	*x/a*	*y/a*	*z*/a	Occupancy	U(Å^{2}x10^3)
B(1)	48(h)	0.0613(2)	0.0613(2)	0.6638(2)	1	6.62
B(2)	48(h)	0.1209(2)	0.1209(2)	0.6832(2)	1	7.03
B(3)	48(h)	0.0864(2)	0.0864(2)	0.5206(2)	1	7.83
B(4)	48(h)	0.1478(2)	0.1478(2)	0.5438(2)	1	8.18
B(5)	48(h)	0.1899(2)	0.1899(2)	0.9098(2)	1	8.17
B,C(6)	48(h)	0.2219(2)	0.2219(2)	0.8378(2)	B/C=0.58/0.42	8.38
B(7)	48(h)	0.1068(2)	0.1068(2)	0.8320(2)	1	5.93
B(8)	48(h)	0.1410(2)	0.1410(2)	0.7596(2)	1	6.85
B(9)	48(h)	0.3018(2)	0.3018(2)	0.4030(3)	1	13.28
B(10)	48(h)	0.2191(2)	0.2191(2)	0.9796(3)	1	11.33
B(11)	48(h)	0.7816(2)	0.7816(2)	0.1217(3)	1	13.61
B(12)	48(h)	0.3019(2)	0.3019(2)	0.4927(3)	1	10.07
B(13)	96(i)	0.7693(2)	0.9520(2)	0.1663(2)	1	14.96
B(14)	48(h)	0.0485(2)	0.0485(2)	0.8212(3)	1	7.51
B(15)	48(h)	0.0340(2)	0.0340(2)	0.1403(3)	1	15.19
B(16)	96(i)	0.7875(2)	0.9762(2)	0.0845(2)	1	16.48
B(17)	48(h)	0.0326(2)	0.0326(2)	0.7384(3)	1	14.68
B,C(18)	16(e)	0.3494(3)	0.3494(3)	0.3494(3)	B/C=0.51/0.49	9.68
B,C(19)	16(e)	0.0623(3)	0.0623(3)	0.0623(3)	B/C=0.85/0.15	12.11
B,C(20)	16(e)	0.4447(2)	0.4447(2)	0.4447(2)	B/C=0.73/0.27	8.9
C(1)	16(e)	0.1947(3)	0.1947(3)	0.1947(3)	1	15.45
Si(1)	4(a)	0.2500(0)	0.2500(0)	0.2500(0)	1	16.19
Si(2)	4(a)	0.5000(0)	0.5000(0)	0.5000(0)	0.38	37.82
Sc(1)	16(e)	0.9409(04)	0.9409(04)	0.9409(04)	1	8.96[a]
Sc(2)	16(e)	0.1270(07)	0.1270(07)	0.1270(07)	0.99	32.99[a]
Sc(3)	48(h)	0.0689(04)	0.0689(04)	0.3216(04)	0.95	11.05[a]

	*U*11	*U*22	*U*33	*U*23	*U*13	*U*12
Sc(1)	8.96	8.96	8.96	-0.91	-0.91	-0.91
Sc(2)	32.99	32.99	32.99	-9.42	-9.42	-9.42
Sc(3)	12.25	12.25	8.65	-0.33	-0.33	-0.12

[a]For Sc sites anisotropic thermal factors are applied and U_{eq} (one-third of the trace of the orthogonarized U_{ij} tensor)is denoted in these columns.

Table 4. Interatomic distances (Å)

B-B bond lengths within B_{12} icosahedra					
B(1)-B(2)	1.757(7)	B(5)-B,C(6)	1.728(7)	B(9)-B(11)	1.814(6)
-B(3)	1.848(5)	-B(7)	1.777(5)	-B(12)	1.821(8)
-B(4)	1.821(4)	-B(8)	1.762(4)	-B(13)	1.868(5)
B(2)-B(2)	1.790(8)	B,C(6)-B,C(6)	1.714(9)	B(10)-B(10)	1.777(11)
-B(4)	1.808(5)	-B(8)	1.739(5)	-B(12)	1.825(5)
B(3)-B(3)	1.890(9)	B(7)-B(7)	1.758(8)	-B(13)	1.772(6)
-B(4)	1.826(7)	-B(8)	1.770(7)	B(12)-B(13)	1.786(5)
B-B bond lengths within B_{10} polyhedron					
B(14)-B(15)	1.873(6)	B(15)-B(15)	1.952(12)	B(17)-B(17)	1.873(12)
-B(16)	1.777(5)	-B(16)	1.801(7)		
-B(17)	1.743(8)	B(16)-B(17)	1.848(6)		
B-B bond lengths for linkages between units					
B(1)-B(17)	1.725(7)	B(2)-B(8)	1.653(7)	B(4)-B(12)	1.778(7)
B(5)-B(10)	1.647(7)	B,C(6)-B,C(6)	1.615(10)	B(7)-B(14)	1.687(7)
B(13)-B(16)	1.772(6)				
B-B bond lengths for linkages between units and bridge sites					
B,C(18)-B(9)	1.747(6)	B,C(19)-B(15)	1.781(6)	B,C(20)-B(3)	1.781(5)
C(1)-B(11)	1.630(6)				
Sc-B and Si-B distances					
Sc(1)-B(14)	2.449(5)	Sc(2)-B(11)	2.628(6)	Sc(3)-B(16)	2.417(5)
-B,C(19)	2.468(6)	-B(15)	2.686(6)	-B,C(18)	2.414(6)
-B(15)	2.561(5)	-B(13)	2.765(4)	-B(17)	2.505(4)
		-C(1)	2.382(10)	-B,C(20)	2.532(6)
				-B(3)	2.631(4)
				-B(1)	2.666(3)
Si(1)-C(1)	1.944(9)	(tetrahedral coordination)			
Si(2)-B,C(20)	1.944(9)	(tetrahedral coordination)			

We think that the above estimations for B/C mixed occupancies on the sites which have shorter bond distances than standard B-B distances are rather reliable because (1) a higher B/C ratio always corresponds to a longer bond distance, (2) the B/C mixed occupancy on any other B sites which have standard B-B distances was denied and (3) the B/C mixed occupancy on the C(1) site which has a much shorter bond distance than other bridging sites was also denied.

The present cubic phase has a homogeneity range which is fairly narrow because the orthorhombic and the hexagonal phases sandwich the range. The composition is still variably dependent on the experimental crystal growth conditions so that we use the expression $Sc_{0.83-x}B_{10.0-y}C_{0.17+y}Si_{0.083-z}$ for the present cubic phase. The number in the suffix of the element is the total number of sites divided by maximum multiplicity of 96 and x and z indicate defects of Sc and Si sites, respectively, and y indicates degrees of mixed occupancy between B and C. For the present crystals x = 0.030, y = 0.36 and z = 0.026 and x = 0.049, y = 0.39 and z = 0.021, respectively.

Site occupancies of three Sc sites are fairly high, 100% for Sc(1), 99% for Sc(2) and 95% for Sc(3), respectively. In the case of second specimen these Sc occupancies are slightly low and 98, 98 and 92%, respectively. One may think from these values that all Sc sites are fully occupied; however, the chemical composition calculated using these values agree better with the measured chemical composition than with the case of fully occupied Sc sites.

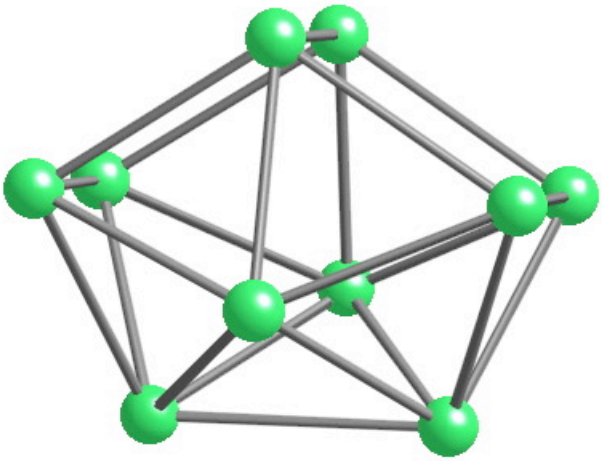

Fig. 2. Newly found B_{10} polyhedron.

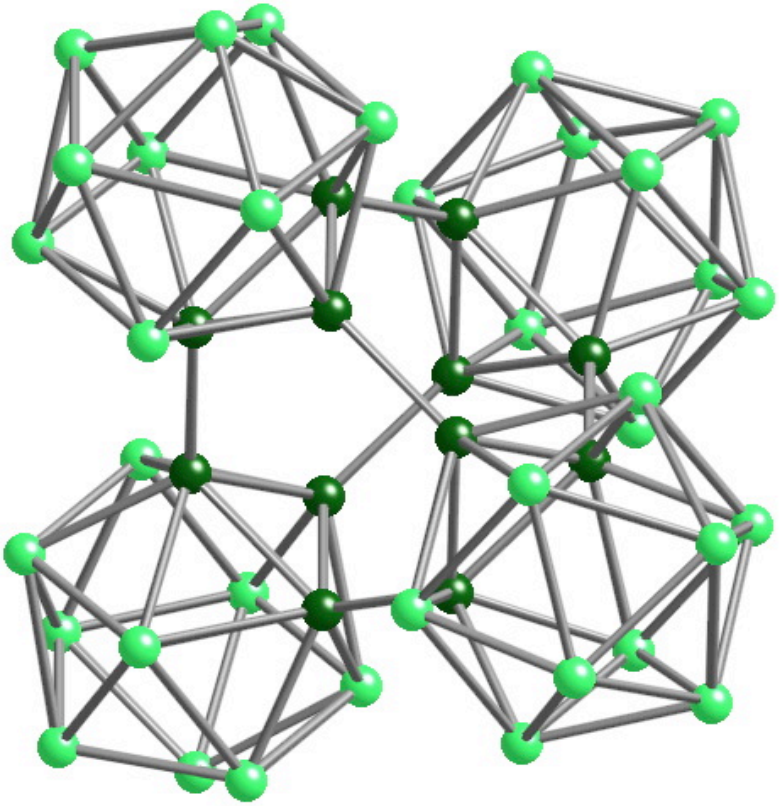

Fig. 3. Super tetrahedron T(2) consists of four icosahedra I(2) and central B,C(6) site's cluster where 7 B atoms and 5 C atoms are accommodated in the case of the first specimen.

Site occupancies of Si(1) and Si(2) are largely different, 100% and only 38%, respectively. Both sites are tetrahedrally coordinated by C(1) sites and B,C(20) sites like SiC and have the same bond length of 1.944(9) Å. The bond length is longer than that (1.883 Å) of SiC. The site occupancy of the Si(2) site for the second specimen is 48%; moreover, bond lengths of the Si(1) and Si(2) sites are 1.935(10) Å and 1.930(10) Å, respectively, which are much shorter than those for the first specimen. Relation between site occupancies and bond distances of the Si sites are not so straightforward like the B/C mixed occupancy cases.

The intraicosahedral and intericosahedral bond distances range from 1.728(7) to 1.890(9) Å and from 1.647(7) to 1.778(7) Å, respectively, excepting for special B,C(6)-B,C(6) bonds previously mentioned. The mean value of the intraicosahedral B-B bond distance 1.793 Å is shorter than the value of 1.813 Å for $ScB_{19+x}Si_y$ [3] and even the value of 1.810 Å for AlB_{10} ($=C_8Al_{2.1}B_{51}$) which is a boron-rich borocarbide phase [11]; however, the variation in the B-B bond distances is comparable with that observed in $ScB_{19+x}Si_y$ (1.725(3) - 1.897(2) Å). The mean value of the intericosahedral B-B bond distance 1.697 Å is much shorter than the value of 1.749 Å for $ScB_{19+x}Si_y$, but is close to the value of 1.709 Å for AlB_{10}. The angles of the triangles of the icosahedra I(1), I(2) and I(3) range from 57.9(2)-61.5(3)°, 59.1(2)-61.1(2)° and 57.9(2)-63.0(3)°, respectively. The variations in the angles of I(1) and I(2) are rather narrow and that of I(3) is comparable with that observed in $ScB_{19+x}Si_y$ (57.0(1)-63.3(1)°) and α-AlB_{12} (57.0(1)-62.0(1)°). The intrabond lengths of the B_{10} polyhedron varies from 1.743(8) to 1.952(12) Å which are wider than those of the icosahedra because of more irregular shape than icosahedra.

3.3. Description of the structure

The crystal structure of $Sc_{0.83-x}B_{10.0-y}C_{0.17+y}Si_{0.083-z}$ is characterized by the presence of a boron framework made up principally of the B_{12} icosahedra and the B_{10} polyhedra as usual boron-rich borides. However, the unit cell includes more than 1000 atoms, it is not so easy to understand the structure on the basis of only the icosahedra and the B_{10} polyhedra. If larger structure units can be categorized, it would be helpful for an easier understanding of the structure.

The super tetrahedron T(2) in which four icosahedra I(2) directly bond each other has already been defined in the previous section. One more super tetrahedron T(1) and a super octahedron O(1) can be categorized; i.e., the super tetrahedron T(1) is formed by four icosahedra I(1), however, in this case these I(1) have no direct bonding but are bridged by four B,C(20) atoms which tetrahedrally surround the Si(2) atom, or we can understand T(1) more easily as that the central Si(2) atom is tetrahedrally coordinated by four B,C(20) atoms and the B,C(20) atom's tetrahedron is further tetrahedrally coordinated by four icosahedra I(1). Each B,C(20) atom has a role to bridge the central Si(2) atom and three outer icosahedra I(2) through the B(3) atoms. The B,C(20) atom locates nearly at the center of a triangle formed by three B(3) atoms.

Fo the super octahedron O(1), the central Si(1) atom is tetrahedrally coordinated by the four C(1) atoms like SiC as mentioned before and the C(1) atom's tetrahedron is octahedrally coordinated by six outer icosahdra I(3). The C(1) atom bridges the Si(1) atom and three

icosahedra I(3). The B,C(18) atom also bridges three icosahedra I(3). Thus, each icosahedron I(3) is doubly connected by both the B,C(18) and C(1) atoms. The super tetrahedron T(1) and the super octahedron O(1) are shown in Figs. 4 (a) and (b), respectively.

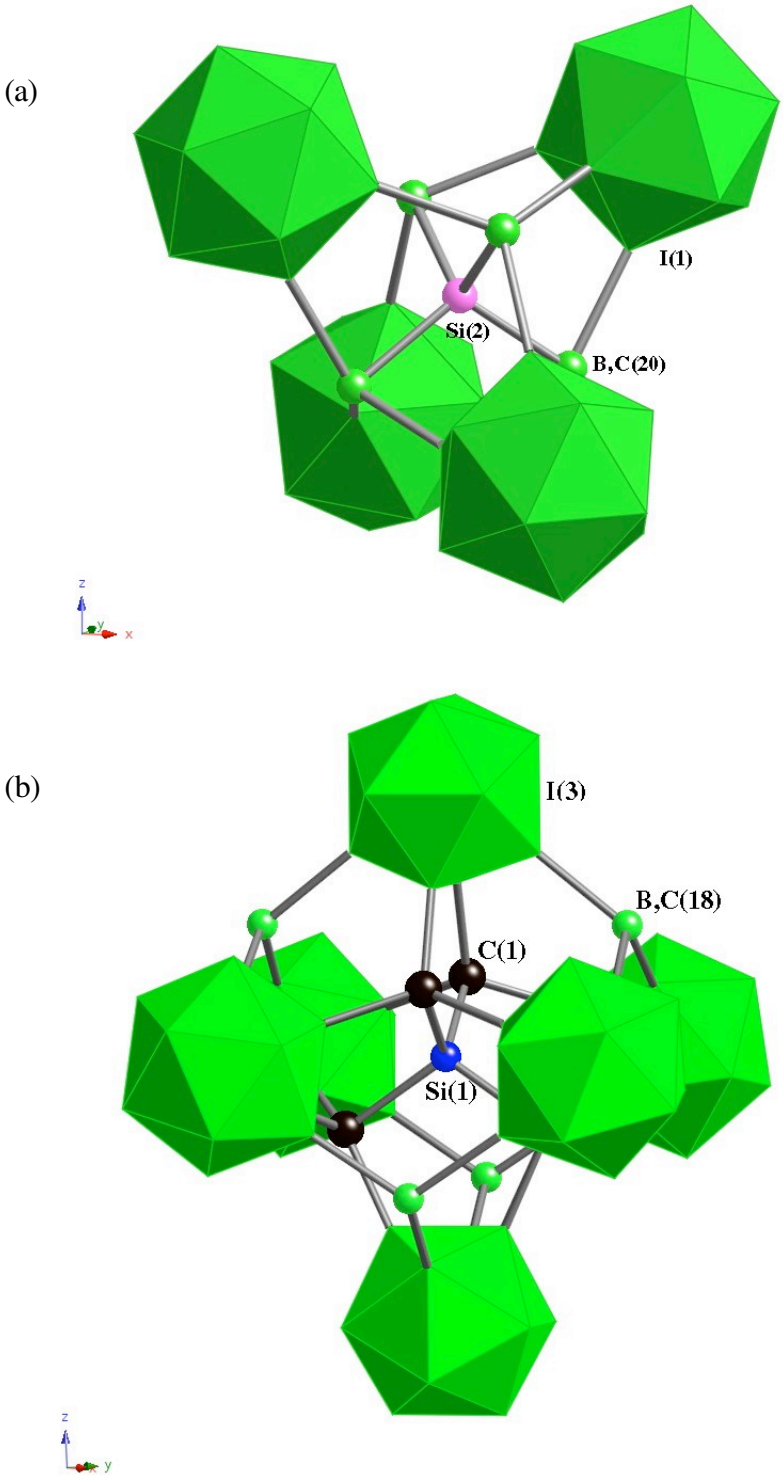

Fig. 4. Details of (a) super tetrahedron T(1) and (b) super octahedron O(1).

Now the boron framework of the $Sc_{0.83-x}B_{10.0-y}C_{0.17+y}Si_{0.083-z}$ structure can be constructed by four structure units of T(1), T(2) and O(1) and the B_{10} polyhedron, where the tetrahedral coordination between these structure units is again a key factor. The super tetrahedron T(1) locates at the body center and the edge center of the cubic unit cell. The super octahedra O(1) which are centered at the symmetry positions of (0.25, 0.25, 0.25) coordinate tetrahedrally surrounding T(1), thus it forms a giant tetrahedron. The super tetrahedron T(2) also surrounds T(1) locating at the symmetry positions of (0.25, 0.25, 0.75) and forms another giant tetrahedron. Edges of both giant tetrahedra orthogonally cross each other at the center of the edges at which each B_{10} polyhedron locates bridging all super structure units T(1), T(2) and O(1). In addition to this bridging role, the B_{10} polyhedron itself forms a super octahedron as shown later in Fig. 6(a) where there is no central atom but each B_{10} polyhedron is bridged by the B,C(19) atom. The super octahedron based on the B_{10} polyhedron is located at each face center lattice point. Thus, the constructed boron lattice is schematically shown in Fig. 5, where the super octahedron based on the B_{10} polyhedron is shown by its original form and others are shown as super structure units T(1), T(2) and O(1).

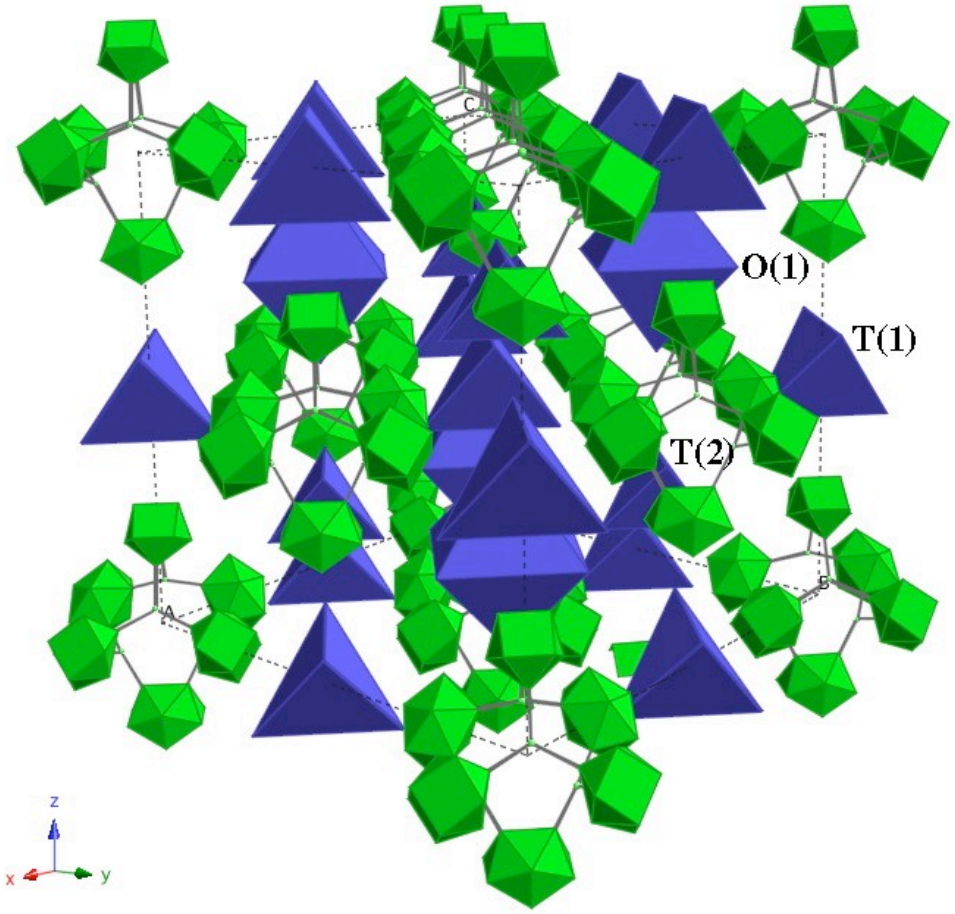

Fig. 5. Boron framework construction by super tetrahedra T(1) and T(2), super octahedra O(1) and the super octahedron based on the B_{10} polyhedron which is shown by its original form. Vertexes of each super polyhedra are adjusted to the center of icosahedra, thus the real volumes of these super polyhedra are slightly larger than those shown here.

Sc atoms reside voids of the boron framework structure. As shown in Fig. 6(a), four Sc(1) sites have a tetrahedral arrangement which crosses another tetrahedral arrangement of the B,C(19) atoms. Both tetrahedra are octahedrally surrounded by B_{10} polyhedra. The B,C(19) atom bridges

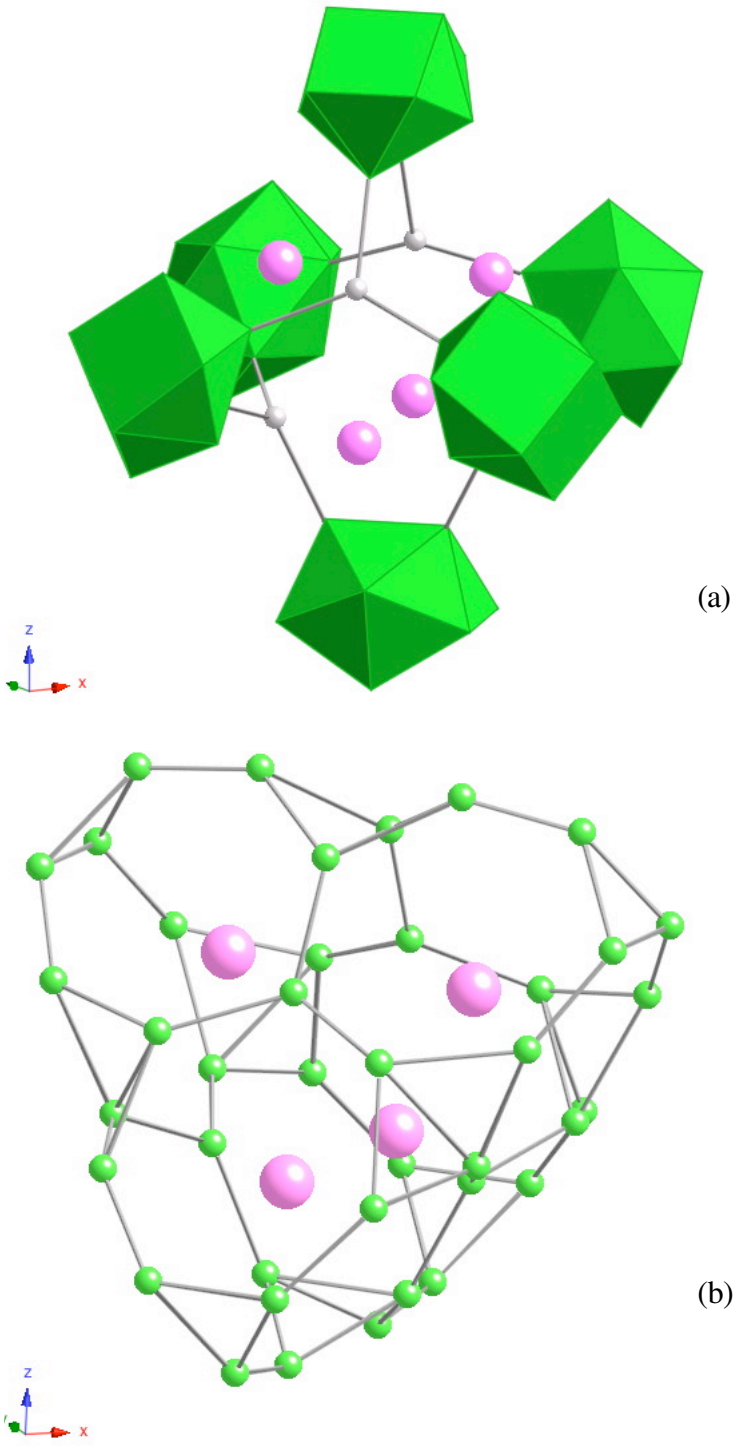

Fig. 6. (a) Sc(1) atom sites form a tetrahedron which is inside of the super octahedron formed by the B_{10} polyhedron and (b) close-up view of four Sc(1) atom sites in a boron framework cage. View direction is same as (a).

three B_{10} polyhedra. The Sc(1) atoms are separated each other by a triangle plane of the B,C(19) atom's tetrahedron, which is necessary because in rare earth boron-rich borides rare earth atoms are expected to be cations by donating their valence electrons to the boron framework bonding. A close up view of the Sc(1) site is shown in Fig. 6(b), where the Sc(1) atom's tetrahedron is in a large boron network cage. The distance between neighbor Sc(1) sites is 3.395 Å.

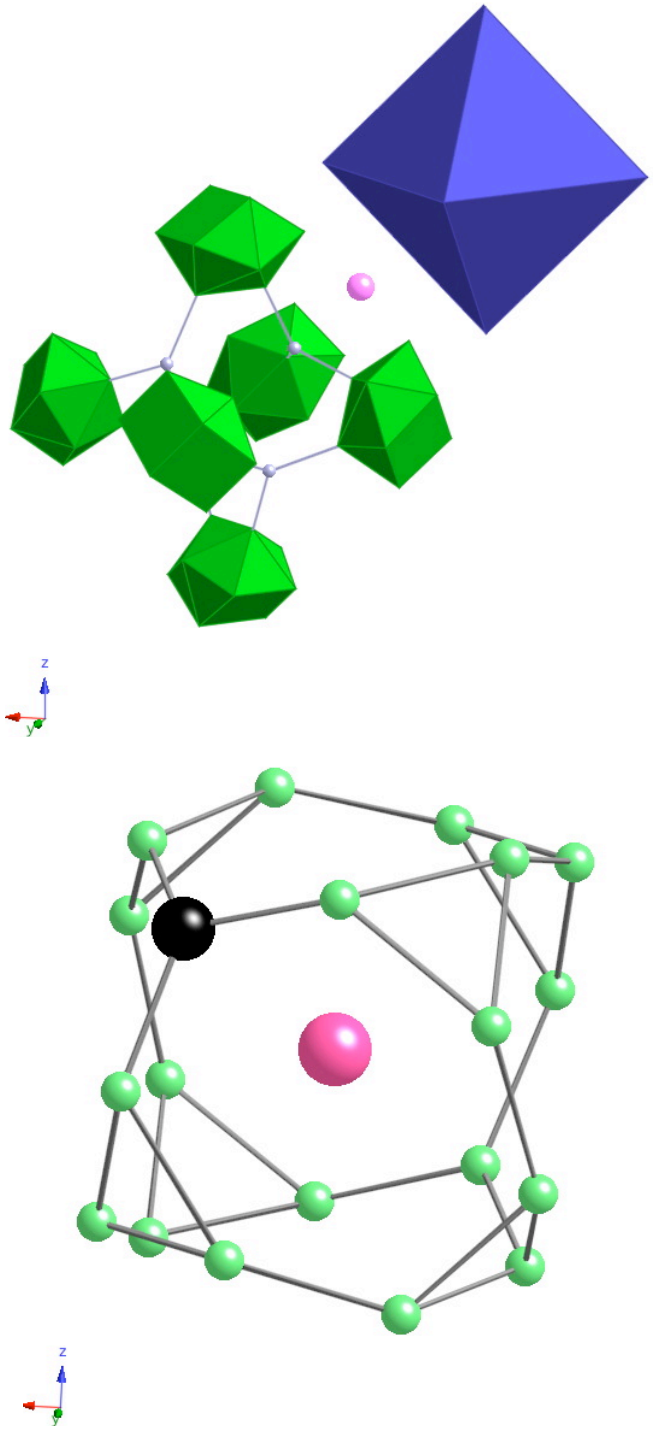

(a)

(b)

Fig. 7. (a) Sc(2) atom site surrounded by three B_{10} polyhedra and one super octahedron O(1) and (b) close up view of the Sc(2) atom site in a boron cage which includes one carbon atom. View direction is same as (a).

The Sc(2) site locates between a triangle plane formed by three B_{10} polyhedra and the super octahedron O(1), as shown in Fig. 7(a). As shown in Fig. 7(b), the Sc(2) atom is in a boron cage which includes one carbon and there is no neighbor Sc site.

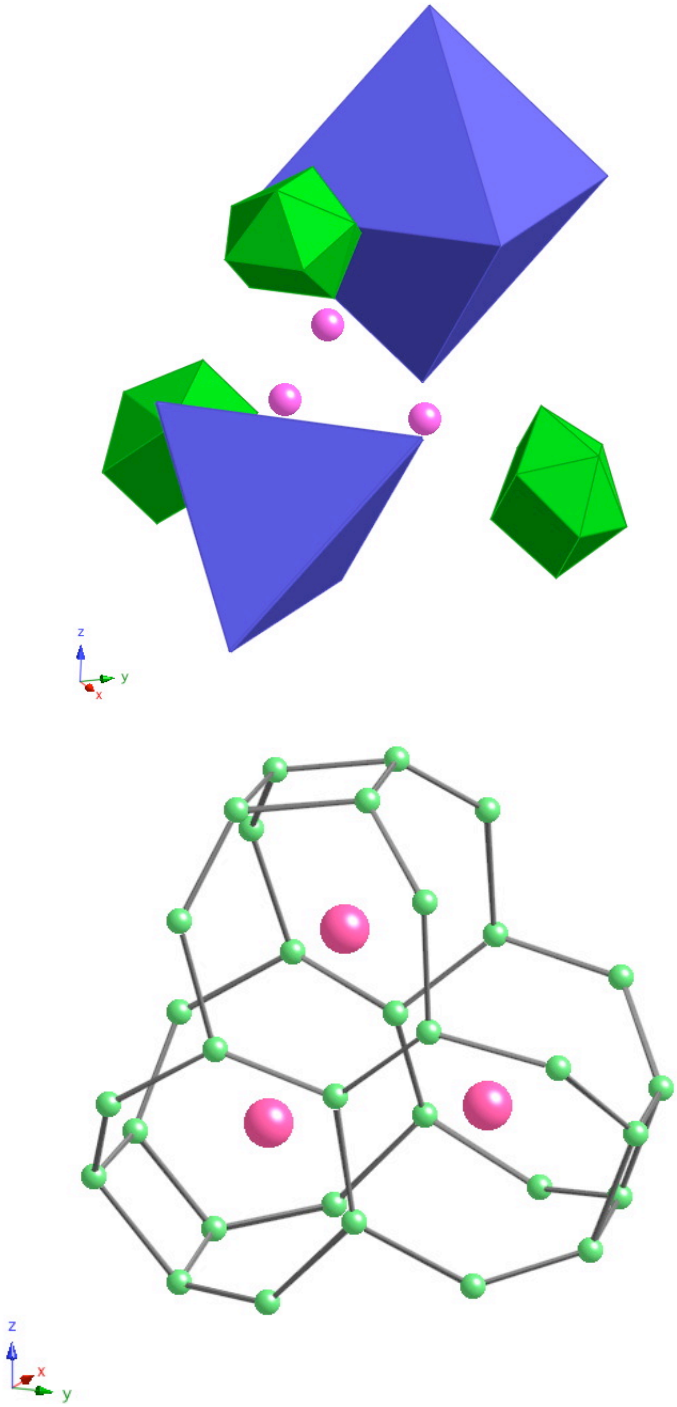

Fig. 8. (a) Sc(3) atom sites form a triangle which is surrounded by three B_{10} polyhedra, a super tetrahedron T(1) and a super octahedron O(1) and (b) close up view of three Sc(3) atom sites in a boron cage. View direction is parallel to the direction from T(1) to O(1).

The Sc(3) site forms a triangle which is surrounded by the super tetrahedron T(1), super octahedron O(1) and three B_{10} polyhedra, as shown in Fig. 8(a). A boron network cage which includes the Sc(3) site's triangle is shown in Fig. 8(b) where the view direction is nearly parallel to a direction from T(1) to O(1). Two central atoms in the figure are the B,C(18) atoms and B,C(20) atoms and atoms connected to them are three B(9) atoms and three B(3) atoms, respectively. The Sc(3) site is separated from the neighbor Sc(3) sites by a rectangular plane formed by the B,C(18), B,C(20), B(3) and B(9) sites. The distance between neighbor Sc(3) site is 3.145 Å.

Preliminary resistivity measurement of not only the cubic phase but also the hexagonal and orthorhombic phases showed that all these phases are semiconductors. The results are consistent with that all previously known B_{12} icosahedral compounds are semiconductors which show variable range hopping-type conduction. On the other hand, ScB_{12} whose B_{12} cluster is a cubo-octahedron is a metal. The compositions of the present phases are very close to ScB_{12} and moreover they include carbon and silicon, but still they stay as semiconductors. Several theoretical calculations of the electronic structure of boron clusters at the 50th year [13] reached a conclusion that the stabilization of each boron cluster needs two more electrons per cluster for all B_6, B_{12} (cubo-octahedron) and B_{12} (icosahedron) to be supplied from metal atoms. The theoretical calculations described well the electronic structure of REB_6 and REB_{12} where rare earth metal atoms are trivalent ions donating two electrons to the boron cluster framework and the remaining one electron behaves as a conduction electron. Thus they are metallic.

On the other hand, for example, the boron framework structure of $REAlB_{14}$ requires four electrons, two electrons for B_{12} and two electrons for two B bridge sites with four bonds. Considering the partial occupancies of both the rare earth atom and the Al atom on their sites, they can donate four electrons if both are trivalent ions [14]. Thus, $REAlB_{14}$ must be a semiconductor. The same electron count is also applicable to $Sc_{0.96}B_{14-y}C_y$ (y=1.1) [15] where 2.9 electrons are necessary to satisfy the closed shell requirement of the boron framework structure which is partly replaced by carbon. Sc could donate just 2.9 electrons if it is assumed to be trivalent. There is an investigation which supports that rare earth atom in the B_{12} icosahedral compounds is trivalent. The result of the structure refinement of YB_{62} [16] suggested that the Y atom is in an ionized state of Y^{3+} because with an increase in valence number, *wR* decreased and the atomic ratio [B]/[Y] approached to 62 which was determined by chemical analysis.

The present scandium borocarbides and borocarbosilicides may be close to metallic conduction because their compositions are close to (B+C)/RE =12. We counted the electrons necessary for attaining the closed shell requirement of the boron framework structure where we assumed that the B_{10} polyhedron also requires two more electrons. Boron polyhedrons require 34.8 electrons per the structural formula listed in Table 1. Since B,C(18) and B,C(19) sites have only three bonds, boron occupation of the sites does not require extra electrons but carbon occupation donates one electron per carbon atom. The B,C(20) site has four bonds so that the boron occupation requires one electron. Thus, total 35.2 electrons are necessary because these bridge sites require only 0.4 electrons per the structural formula. On the other hand, Sc atoms

could donate 57.9 electrons if they are trivalent, resulting that about 23 electrons per formula unit (= 91 electrons/unit cell or 1.2 electrons/Sc) remain. This seems to be an unrealistic result, suggesting that the Sc atoms in the present compound has lower valence states than Sc^{3+}.

In fact, Sc-Sc distances of the Sc(1) and Sc(3) sites mentioned above are comparable with those (3.309 Å and 3.256 Å) of Sc metals and further they are surrounded by the boron cage. More covalent character should be considered for the bonding between the Sc atoms and the boron framework structure, which would reduce valence of the Sc atoms. X-ray photoelectron spectroscopy measurement was carried out in order to estimate the valence state of the Sc atom. The measured binding energy of Sc $2p^{3/2}$ was 399.7 eV which lies between that (399 eV) for the Sc metal and that (401.8 eV) for Sc_2O_3, which is consistent with the above expectation that the valence state of the Sc atoms in the present compound is intermediate between them.

4. Concluding remarks

The FZ-grown single crystals of the present novel compound had compositions of about $ScB_{12.7}C_{0.62}Si_{0.08}$, meanwhile the most reliable composition of the compound synthesized by solid-state reaction has been $ScB_{15}C_{0.8}$. The difference of Sc/B ratio between them is probably due to the difference of Sc site occupancies which are dependent on the synthesis conditions.

Composition control for single-crystal growth of the quaternary compound was not so easy. Partition behaviors of carbon and silicon are opposite, carbon acts to increase the melting temperature and silicon reduces. Silicon preferentially evaporates from the molten zone than other elements, which required to add excess silicon in the feed rod to compensate the evaporation loss. Moreover, single-crystal growth itself was fairly difficult and seemed to be closer to the flux growth than the melt growth. The grown crystals used to include many grains and even cracks. Another difficulty of this cubic phase was the appearance of two very close neighbor phases, i.e., the hexagonal $ScB_{11.7}C_{0.6}Si_{0.04}$ phase and the orthorhombic $ScB_{12.8}C_{0.7}Si_{0.004}$ phase. Phase and structure correlation between them must be subjects for further investigations.

The face-centered cubic structure of the present $Sc_{0.83-x}B_{10.0-y}C_{0.17+y}Si_{0.083-z}$ is a new structure type of rare earth boron-rich borides and the B_{10} polyhedron found in the structure is a new polyhedron type of boron-rich borides.

Acknowledgments

The authors thank Mr. S. Takenouchi for chemical analysis, Mr. K. Kosuda for EPMA measurements and Dr. S. Suehara for XPS measurement, respectively. They also thank Dr. I. Higashi of Chiba Institute of Technology for useful discussions on crystal structure analysis.

References

1. Y. Shi, A. Leithe-Jasper and T. Tanaka, *J. Solid State Chem.* **148**, 250 (1999)
2. T. Tanaka, S. Okada and V. N. Gurin, *J. Alloys Comp*. **267**, 211 (1998)
3. T. Tanaka and A. Sato, *J. Solid State Chem*. **160**, 394 (2001)

4. T. Tanaka, *J. Alloys Comp*. **270**, 132 (1998)
5. A. Leithe-Jasper, L. Bourgeois, Y. Michiue, Y. Shi and T. Tanaka, *J. Solid State Chem*. **154**, 130 (2000)
6. A. Leithe-Jasper, A. Sato and T. Tanaka, *Z. Kristalogr*. NCS **216** 45 (2000)
7. T. Tanaka, S. Okada and Y. Ishizawa, *J. Solid State Chem*. **133**, 55 (1997)
8. A. Altomare, G. Cascarano, C. Giacovazzo, A. Guagliardi, M. Burla, G. Polidori and Camalli, *J. Appl. Cryst.* **27**, 435 (1994)
9. G. M. Sheldrick, SHELX97: a program for the solutin and refinement of crystal structures, Universität Göttingen, Göttingen, Germany 1997
10. D. Palmer, *CrystalMaker* vers. 4.1.4, CrystalMaker Software, Bicester, Oxfordshire, OX6 7BS, UK.
11. T. Tanaka and A. Sato, *J. Solid State Chem*. **160**, 394 (2001)
12. G. Will, *Acta Crystallogr*. **23**, 1071 (1967)
13. W. N. Lipscomb and D. Britton, *J. Chem. Phys.* **33**, 275 (1960), H. C. Longuet-Higgins and M. deV Roberts, *Proc. Roy. Soc. London*, **A224**, 336 (1954), ibid., *Proc. Roy. Soc. London*, **A230**, 110 (1955), M. Yamazaki, *J. Phys. Soc. Jap*. **12**, 1 (1957) and S. Flodmark, *Ark. Fys*. **14**, 513 (1959).
14. M. Korsukova and V. N. Gurin, *J. Alloys Comp*. **187**, 39 (1992).
15. A Leithe-Jasper, A. Sato and T. Tanaka, *Z. Kristallogr. NCS* **216**, 45 (2001)
16. I. Higashi, K. Kobayashi, T. Tanaka and Y. Ishizawa, *J. Solid State Chem.* **133**, 16 (1997)